Large anomalous Hall effect and spin Hall effect by spin-cluster scattering in the strong-coupling limit

Hiroaki Ishizuka and Naoto Nagaosa

Phys. Rev. B **103**, 235148 — Published 23 June 2021

DOI: 10.1103/PhysRevB.103.235148

Large anomalous Hall effect and spin Hall effect by spin-cluster scattering in the strong-coupling limit

Hiroaki Ishizuka[1,*] and Naoto Nagaosa[2,3]

[1] *Department of Physics, Tokyo Institute of Technology, Meguro, Tokyo, 152-8551, JAPAN*
[2] *Department of Applied Physics, The University of Tokyo, Bunkyo, Tokyo, 113-8656, JAPAN*
[3] *RIKEN Center for Emergent Matter Sciences (CEMS), Wako, Saitama, 351-0198, JAPAN*

(Dated: June 11, 2021)

Skew scattering — an asymmetric scattering of electrons by impurities — is one of the major mechanisms causing anomalous/spin Hall effects. While many microscopic mechanisms for skew scattering are known, the Hall angle of anomalous Hall effect by these mechanisms is often small, typically $\theta = 0.1^\circ - 1^\circ$. In this work, we study the skew scattering by three-spin clusters focusing on the strong Kondo coupling regime. Using a T-matrix formalism, we calculate the scattering probability for arbitrary strength of Kondo coupling, going beyond perturbation theory in previous studies. From a systematic analysis of the scattering probability for one-, two-, and three-spin clusters, we show that three spins are necessary for the skew scattering in the absence of spin-orbit interaction. The skew scattering by three-spin cluster produces a skew angle of order 0.1π rad ($\sim 18^\circ$) when the electron-spin coupling is comparable to the bandwidth. We also study the relationship between anomalous/spin Hall effects and the spin chiralities, and argue that the anomalous-(spin-)Hall skew angle is approximately proportional to the scalar (net vector) spin chirality even for the strong coupling cases. This mechanism is potentially relevant to anomalous/spin Hall effects in noncentrosymmetric and frustrated magnets.

I. INTRODUCTION

Anomalous and spin Hall effects reflect rich physics related to the quantum nature of electrons such as Berry phase and electron scattering by impurities [1–3]. Traditionally, the microscopic mechanisms of the Hall effects are classified into two groups: intrinsic and extrinsic mechanisms. The intrinsic mechanism of the anomalous Hall effect (AHE) [4] is related to the Berry curvature of electronic bands [5]. Later it was realized that the same mechanism also produces spin Hall effect (SHE) [6, 7]. More recently, it was pointed out that the scalar spin chirality of ordered localized spins also contributes to the AHE [8–10]. This mechanism is thought to be responsible for the intrinsic AHE in ordered phases of magnets with non-coplanar magnetic order, such as in pyrochlore [11] and kagome [12] magnets, and in chiral magnets [13, 14]. On the other hand, the extrinsic mechanisms of AHE are related to impurity scattering. Several mechanisms are known for single non-magnetic [15, 16] or magnetic [17–19] impurities; they also contribute to the SHE [20, 21]. While a variety of mechanisms are known, in three-dimensional materials, the Hall angle of anomalous Hall conductivity $\sigma_{xy}^{(\mathrm{AHE})}$ is usually small compared to the longitudinal conductivity σ_{xx}. Typically $\sigma_{xy}^{(\mathrm{AHE})}/\sigma_{xx} = 10^{-3} - 10^{-2}$ regardless of the mechanism [23].

In extrinsic mechanisms, the small Hall angle is related to the spin-orbit interaction necessary for all extrinsic mechanisms by a single impurity. An example is skew scattering in ferromagnets, in which the electrons are scattered asymmetrically by the spin-orbit interaction of an impurity. This effect, however, is often a weak perturbation compared with the energy scale of the hybridization between the resonance state and the conduction electrons. Hence, limiting the skew angle.

In contrast, such limitation does not apply to the skew scattering by multiple spins [8, 9, 24], which occurs without spin-orbit interaction. With small Kondo coupling, the AHE is directly related to the scalar spin chirality of impurity spins [24],

$$\boldsymbol{S}_i \cdot (\boldsymbol{S}_j \times \boldsymbol{S}_k); \tag{1}$$

here, $\boldsymbol{S}_{i,j,k}$ are three spins adjacent to each other. Later, it was shown that this AHE, in good metals, originates from a skew scattering by three-spin clusters [25, 26]. In addition, a mechanism related to the vector spin chirality also contributes to the AHE [27–30]. This mechanism may produce a large skew angle because the strong coupling between electrons and spins is often realized in transition-metal materials, e.g., in Mn compounds [35, 42]. However, most theoretical studies so far focus on the weak-coupling limit, except for a few numerical works [28, 31–33].

In this work, we study the skew scattering by multiple spins described by Anderson impurities using a T-matrix method [Fig. 1(a)]. This method allows calculation beyond the weak-coupling limit studied in related works [24, 30]. Using this method, we find that the skew angle reaches the order of 0.1π rad when the electron-spin coupling is comparable to the bandwidth; this skew angle is 10-100 times larger than the typical skew angle. We also argue that the skew angles for AHE/SHE behave similarly to the spin chiralities, and hence, the chiralities function as an indicator for AHE/SHE at arbitrary Kondo coupling [24, 30]. On the experimental side, the

* ishizuka@phys.titech.ac.jp

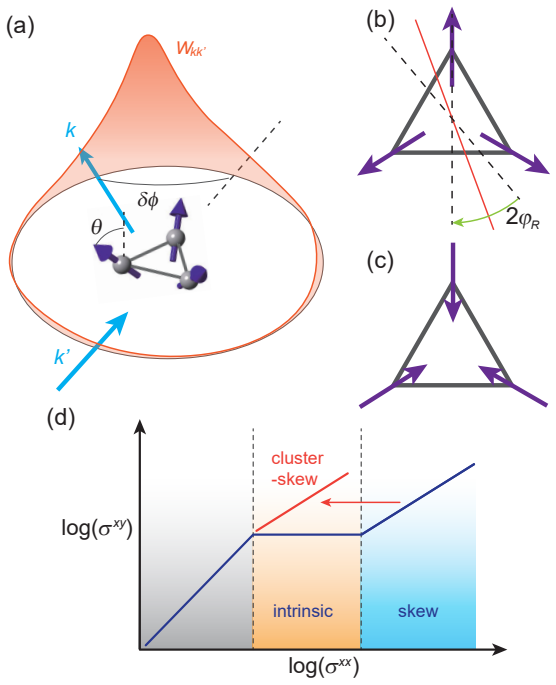

FIG. 1. Schematic figure of a three-spin cluster and skew scattering. (a) Schematic figure of the electron scattering by a three-spin cluster. The blue arrows show the incoming ($\boldsymbol{k}'$) and outgoing ($\boldsymbol{k}$) electrons and the orange curve surrounding the spin cluster is the scattering rate $W_{\boldsymbol{k}\boldsymbol{k}'}$ for the outgoing electrons for $\boldsymbol{k}'$; we abbreviate the spin indices of the electrons. The skew scattering makes the scattering rate asymmetric with respect to the incident direction shown by the dashed line. θ in (a) is the canting angle of the three spins. (b) and (c) are respectively the top view of the three-spin cluster canted outward (b) and inward (c). See the main text for details. (d) Schematic figure of the scaling relation of anomalous Hall effect.

large skew angle may modify the scaling plot of AHE; a large skew-scattering AHE extends the skew-scattering region to lower conductivity. In the extreme case, the skew-scattering region completely mask the intrinsic region as shown by the red line when the Hall angle reaches 0.1π rad. We also discuss that the spin cluster scattering produces a large spin Hall angle, which is related to the net vector spin chirality of three pairs of spins consisting the cluster. The T-matrix analysis implies that the magnetic scattering in the strong-coupling region can produce a large AHE/SHE by skew scattering which are approximately proportional to scalar/vector spin chiralities.

II. MODEL AND METHOD

We study the T matrix of a triangular lattice model with three impurity sites subject to the Zeeman field. The Hamiltonian is

$$H = H_f + H_c + H_{fc} + H_{cf}, \tag{2a}$$

$$H_f = -J \sum_{i=0,1,2} \boldsymbol{S}_i \cdot f_i^\dagger \boldsymbol{\sigma} f_i, \tag{2b}$$

$$H_c = \sum_{\boldsymbol{k}} \varepsilon_{\boldsymbol{k}} c_{\boldsymbol{k}}^\dagger c_{\boldsymbol{k}}, \tag{2c}$$

$$H_{fc} = -\frac{V}{\sqrt{N}} \sum_{\substack{i=0,1,2 \\ \boldsymbol{k},\sigma}} \gamma_{i\boldsymbol{k}} f_{i\sigma}^\dagger c_{\boldsymbol{k}\sigma}, \tag{2d}$$

$$H_{cf} = -\frac{V}{\sqrt{N}} \sum_{\substack{i=0,1,2 \\ \boldsymbol{k},\sigma}} \gamma_{i\boldsymbol{k}}^* c_{\boldsymbol{k}\sigma}^\dagger f_{i\sigma}, \tag{2e}$$

where $c_{\boldsymbol{k}\sigma}$ and $f_{i\sigma}$ ($c_{\boldsymbol{k}\sigma}^\dagger$ and $f_{i\sigma}^\dagger$) are respectively the annihilation (creation) operator of itinerant and localized electrons, $\vec{\sigma} \equiv (\sigma^x, \sigma^y, \sigma^z)$ is the vector of Pauli matrices σ^a ($a = x, y, z$), $c_{\boldsymbol{k}} = (c_{\boldsymbol{k}\uparrow}, c_{\boldsymbol{k}\downarrow})$ [$f_i = (f_{i\uparrow}, f_{i\downarrow})$] is the spinor for itinerant (localized) electrons,

$$\begin{aligned}\varepsilon_{\boldsymbol{k}} &= -2t \left[\cos(k_x) + 2\cos\left(\frac{k_x}{2}\right) \cos\left(\frac{\sqrt{3}k_y}{2}\right) \right] - \mu, \\ &\sim -(6t + \mu) + \frac{3}{2} t k^2,\end{aligned} \tag{3}$$

is the eigenenergy of itinerant electrons on the triangular lattice with momentum $\boldsymbol{k}$, $k \equiv |\boldsymbol{k}|$, $\gamma_{i\boldsymbol{k}} \equiv e^{i\boldsymbol{k}\cdot\boldsymbol{r}_i}$, $J > 0$ is the Zeeman splitting of the localized electron, V is the hybridization of itinerant (c) and localized (f) electrons, $\boldsymbol{r}_i$ is the position of ith spin, and $\vec{S}_i$ is a unit vector parallel to the localized spin on site i. Here, we assumed the site distance $a = 1$. The eigenenergy of electrons are approximated by a quadratic dispersion. This model corresponds to a mean-field theory for the Anderson impurity model, where the onsite interaction between the localized electrons are treated by Hartree-Fock approximation. Note that there is no spin-orbit interaction in Eq. (2a).

We calculate the scattering rate using a T-matrix method. The details of derivation are in the Appendix. We here summarize the main results we use in the rest of this paper. The T matrix for the spin cluster above reads

$$T_{\boldsymbol{k}\sigma,\boldsymbol{k}'\sigma'} = \frac{V^2}{N} \sum_{i,j} \gamma_{i\boldsymbol{k}}^* \gamma_{j\boldsymbol{k}'} \left[\frac{1}{\varepsilon + i\delta + J \sum_l \boldsymbol{S}_l \cdot \boldsymbol{\sigma}_l - \Sigma(\varepsilon)} \right]_{i\sigma,j\sigma'}, \tag{4}$$

where $\Sigma(\varepsilon)$ is the self-energy whose elements are

$$\Sigma_{i\sigma,j\sigma'}(\varepsilon) = \frac{V^2}{4\pi^2} \delta_{\sigma\sigma'} \int d\boldsymbol{k} \, \frac{\gamma_{i\boldsymbol{k}} \gamma_{j\boldsymbol{k}}^*}{\varepsilon + i\delta - \varepsilon_{\boldsymbol{k}}}. \tag{5}$$

Using the T matrix, the scattering rate from a state with $\boldsymbol{k}'$ and spin σ' to that with $\boldsymbol{k}$ and σ reads,

$$W_{\vec{k}\sigma,\vec{k}'\sigma'} = 2\pi \mathcal{W}_{\vec{k}\sigma,\vec{k}'\sigma'} \delta(\varepsilon_{\vec{k}\sigma} - \varepsilon_{\vec{k}'\sigma'}), \tag{6}$$

where $\mathcal{W}_{\vec{k}\sigma,\vec{k}'\sigma'} \equiv |T_{\vec{k}\sigma,\vec{k}'\sigma'}|^2$.

We study the skew scattering by spin clusters using the average of $\mathcal{W}_{\boldsymbol{k}\sigma,\boldsymbol{k}'\sigma'}$ over the incident electron directions, defined by

$$\begin{aligned}\bar{\mathcal{W}}_{\sigma,\sigma'}(\delta\phi) \equiv& \int \frac{d\phi'}{2\pi}\mathcal{W}_{\boldsymbol{k}\sigma,\boldsymbol{k}'\sigma'}, \\ =&\frac{V^4}{N^2}\sum_{i,j,m,n}\left[\frac{1}{J\sum_l \boldsymbol{S}_l\cdot\boldsymbol{\sigma}_l - \Sigma(\varepsilon)}\right]_{i\sigma,j\sigma'}\left[\frac{1}{J\sum_l \boldsymbol{S}_l\cdot\boldsymbol{\sigma}_l - \Sigma(\varepsilon)}\right]^*_{m\sigma,n\sigma'} \\ &\times J_0\left(k\sqrt{r_{jn}^2 + r_{im}^2 - 2\boldsymbol{r}_{im}\cdot\boldsymbol{r}_{jn}\cos(\delta\phi) + 2(\boldsymbol{r}_{im}\times\boldsymbol{r}_{jn})_z\sin(\delta\phi)}\right), \end{aligned} \tag{7}$$

where $\boldsymbol{r}_{ij} \equiv \boldsymbol{r}_i - \boldsymbol{r}_j$, $\phi' \equiv \mathrm{atan}(k'_y/k'_x)$ is the angle of incident electron, $\delta\phi$ is the difference of angles between the momentum of incoming and outgoing electrons, $\vec{\sigma}_l \equiv (\sigma_l^x, \sigma_l^y, \sigma_l^z)$ is a vector of matrix $\sigma_l^a \equiv E_{ll}\otimes\sigma^a$ ($a = x, y, z$ and E_{ij} is the matrix unit), and $J_0(x)$ is the $n = 0$ first Bessel function, $J_0(x) = \sum_{n=0}^{\infty}\frac{(-1)^n}{(n!)^2}\left(\frac{x}{2}\right)^{2n}$. Using Eq. (7), the averaged scattering rate reads

$$\bar{W}_{\sigma,\sigma'}(\delta\phi) = 2\pi\bar{\mathcal{W}}_{\sigma,\sigma'}(\delta\phi)\delta(\varepsilon_{\vec{k}\sigma} - \varepsilon_{\vec{k}'\sigma'}). \tag{8}$$

We first look at skew scattering in one- and two-impurity cases. In the case of one impurity, $\boldsymbol{r}_{11} = 0$. Hence, no asymmetry in $\bar{\mathcal{W}}_{\boldsymbol{k}\sigma,\boldsymbol{k}'\sigma'}$. To consider the two-impurity case, suppose the impurities are placed with a distance r; $r_{ij} = 0$ if $i = j$ and $r_{ij} = r$ otherwise. The cross product in Eq. (7) vanishes in this case, becoming

$$\bar{\mathcal{W}}_{\vec{k}\sigma,\vec{k}'\sigma'} = \frac{V^4}{N^2}\sum_{i,j,m,n}\left[\frac{1}{J\sum_l \vec{S}_l\cdot\vec{\sigma}_l - \Sigma(\varepsilon)}\right]_{i\sigma,j\sigma'}\left[\frac{1}{J\sum_l \vec{S}_l\cdot\vec{\sigma}_l - \Sigma(\varepsilon)}\right]^*_{m\sigma,n\sigma'} J_0\left(k\sqrt{r_{jn}^2 + r_{im}^2 - 2\vec{r}_{im}\cdot\vec{r}_{jn}\cos(\delta\phi)}\right) \tag{9}$$

Therefore, $\bar{\mathcal{W}}_{\boldsymbol{k}\sigma,\boldsymbol{k}'\sigma'} = \bar{\mathcal{W}}'_{\sigma,\sigma'}(\delta\phi)$ is always symmetric with respect to $\delta\phi$. Hence, we need at least three spins for skew scattering.

III. LARGE SKEW SCATTERING BY THREE-SPIN CLUSTER

Previous studies find a three-spin cluster causes skew scattering [25, 26] and AHE [24–26]. These works use a perturbation expansion with respect to the Kondo coupling, which is valid when the Kondo coupling is small compared to the Fermi energy. In contrast, we here study the behavior of electron scattering using a formalism valid for arbitrary strength of electron-spin coupling.

For concreteness, we consider a three-spin cluster consisting of three nearest-neighbor sites on the triangular lattice. The scattering rate for an umbrella configuration with the canting angle $\theta = \pi/4$ [Fig. 1(a)] is shown in Fig. 2(a). The result is asymmetric with respect to $\delta\phi$, indicating skew scattering. As a measure of skewness, we calculate the skew angle defined by

$$\delta\bar{\phi}_\sigma = \int_{-\pi}^{\pi}\frac{d(\delta\phi)}{\Omega_\sigma}\,\delta\phi\bar{\mathcal{W}}_{\sigma,\sigma}(\delta\phi), \tag{10}$$

where $\Omega_\sigma = \int_{-\pi}^{\pi} d(\delta\phi)\,\bar{\mathcal{W}}_{\sigma,\sigma}(\delta\phi)$. Figures 2(b) and 2(c) shows the Fermi wavenumber k_F dependence of $\delta\bar{\phi}_\sigma$ for $J = V$ cases. The results for $\delta\bar{\phi}_\uparrow$ and $\delta\bar{\phi}_\downarrow$ looks alike when the coupling is weak ($J/t = V/t = 1$), i.e., the sign of $\delta\bar{\phi}_\sigma$ is negative and the minimum is at around $k_F \sim 1.5$. This behavior is approximately consistent with the perturbation theory in Ref. [26], in which $\bar{\mathcal{W}}_{\uparrow,\uparrow}(\delta\phi) = \bar{\mathcal{W}}_{\downarrow,\downarrow}(\delta\phi)$. On the other hand, $\delta\bar{\phi}_\uparrow$ and $\delta\bar{\phi}_\downarrow$ behaves differently for large $J/t, V/t$. For instance, the sign of $\delta\bar{\phi}_\uparrow$ is positive and $\delta\bar{\phi}_\downarrow$ is negative when $J/t = V/t = 10$, resembling the fictitious magnetic-field argument in the double-exchange limit [8, 9].

The average skew angle reaches $\delta\bar{\phi}_\sigma = \mathcal{O}(0.1\pi)$ in between the weak and strong coupling limits, such as in $J/t, V/t \gtrsim 5$. This is 10-100 times larger than the typical skew angle $\delta\bar{\phi}_\sigma \sim 10^{-3}\pi - 10^{-2}\pi$ rad [1]. Such a large skew angle appears for a wide range of canting angle $\pi/5 \le \theta \le 4\pi/5$ as in Fig. 3, demonstrating that

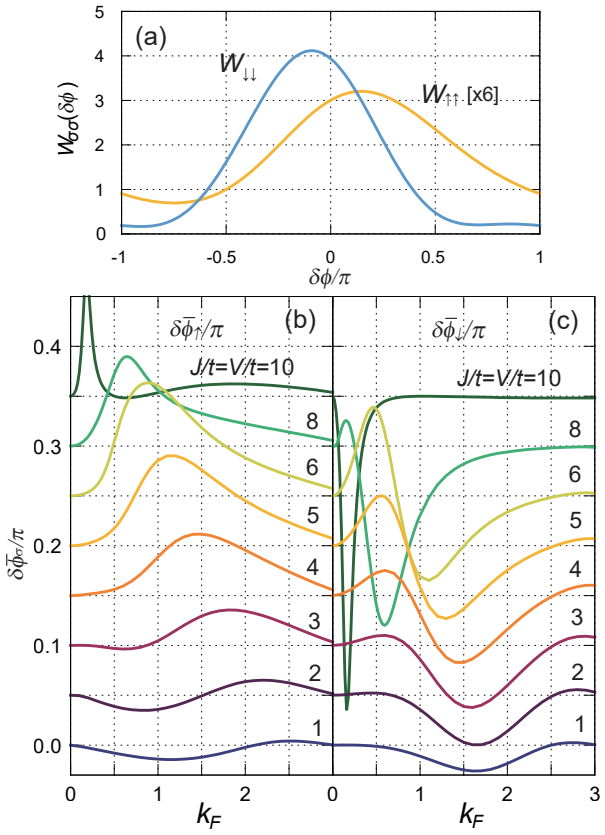

FIG. 2. Scattering rate and skew angle for three-spin cluster. (a) $\delta\phi$ dependence of $\bar{\mathcal{W}}_{\uparrow,\uparrow}(\delta\phi)$ and $\bar{\mathcal{W}}_{\downarrow,\downarrow}(\delta\phi)$ for $J = V = 6$, $k_F = 1$, and $\theta = \pi/4$. (b,c) k_F dependence of (b) $\delta\bar{\phi}_\uparrow$ and (c) $\delta\bar{\phi}_\downarrow$ for $\theta = \pi/4$. Different curves are for different J and V. The unit of k_F is the inverse of the bond length a, and the cutoff is $\Lambda = \pi$.

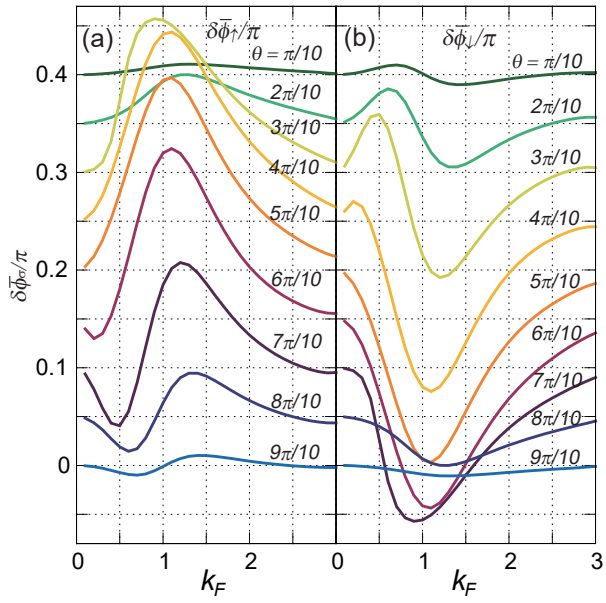

FIG. 3. Canting dependence of the skew angle. k_F dependence of (a) $\delta\bar{\phi}_\uparrow$ and (b) $\delta\bar{\phi}_\downarrow$ for different canting angles θ with $J/t = V/t = 5$. The transverse axis is the Fermi wavenumber k_F.

a large skew angle appears generally with strong Kondo coupling.

To connect the skew angle to AHE, we look at the spin-configuration dependence of the average of $\delta\bar{\phi}_{\uparrow,\downarrow}$, $\delta\bar{\phi}^+ \equiv (\delta\bar{\phi}_\uparrow + \delta\bar{\phi}_\downarrow)/2$. The result is shown in Fig. 4(a), where θ and φ correpond to the angles in Figs. 4(c) and 4(d). The contour plot resembles scalar spin chirality in Fig. 4(b); they are both antisymmetric about $\theta = 1/2$ and $\varphi = \pi$ lines, and the maximum in each quadrant is approximately at the same point. The resemblance implies a close relation between scalar spin chirality and AHE even for a large $J/t, V/t$.

We next turn to the magnitude of $|\delta\bar{\phi}_\sigma|$, which shows maximum at $k_F \sim 1$. The position of the maximum resembles magnon scattering by skyrmions, in which the maximum is at a wavenumber comparable to the inverse of the skyrmion diameter [36]. Reference [36] also points out that a theory for electron scattering by Aharonov-Bohm flux [37–39] reproduces the numerical simulation of magnon scattering. Our model shares a similar aspect to the magnon scattering problem; the coupling of electrons to localized moments reduces to a fictitious magnetic field in the strong Kondo-coupling limit [8, 9]. Hence, the peak at $k_F \sim 1$ is likely to be related to the spin cluster size.

In the last, we discuss the impact of the large skew angle on the scaling plot. Figure 1(d) is the schematic figure of the scaling plot of the anomalous Hall effect. In ferromagnets, the Hall conductivity shows three distinct behaviors depending on the longitudinal conductivity [22, 23]. The conventional skew scattering is seen only in the clean limit with conductivity $\sigma_{xx} \gtrsim 10^5\Omega^{-1}\mathrm{cm}^{-1}$ [the right region in Fig. 1(d)], while intrinsic Hall effect is dominant for $10^3 \lesssim \sigma_{xx} \lesssim 10^5\Omega^{-1}\mathrm{cm}^{-1}$. This crossover is a consequence of two different scaling behaviors. When the skew scattering is dominant, σ_{xy} obeys the skew-scattering scaling relation $\sigma_{xy} \propto (\sigma_{xx})^1$, while the scaling becomes $\sigma_{xy} = (\sigma_{xx})^0$ when the intrinsic one is dominant. This crossover often takes place at $\sigma_{xx} \sim 10^5\Omega^{-1}\mathrm{cm}^{-1}$ [22, 23] because σ_{xy} for intrinsic AHE is $\sigma_{xy} \sim 10^3\Omega^{-1}\mathrm{cm}^{-1}$ while the Hall angle for skew scattering is $\sigma_{xy}/\sigma_{xx} = 0.01 - 0.001$. For a large skew-scattering Hall effect, the skew-scattering region extends to the lower σ_{xx} owing to a larger Hall angle [40]. As the intrinsic region spans between $10^3 \lesssim \sigma_{xx} \lesssim 10^5\Omega^{-1}\mathrm{cm}^{-1}$, the skew scattering may completely mask the intrinsic region if the magnitude increases more than an order of magnitude [Fig. 1(d)].

IV. SPIN-HALL EFFECT BY SPIN-CLUSTER SCATTERING

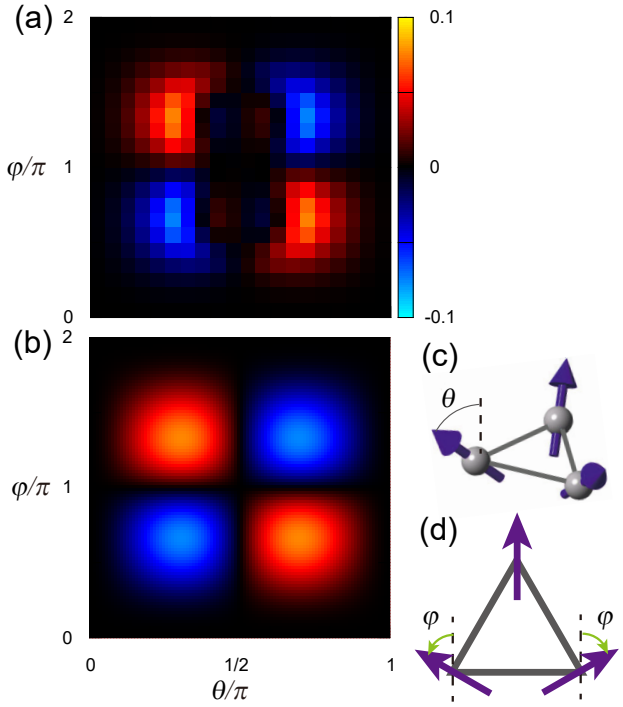

FIG. 4. Spin configuration dependence of the average skew angle $\delta\bar{\phi}^{+}$. (a) Contour plot of $\delta\bar{\phi}^{+}/\pi$ calculated using Eq. (7) and (b) the net scalar spin chirality with $\varphi_2 = \pi/2$. (a) is the result for $J/t = V/t = 6$, $k_F = 1/2$, and $\theta = \pi/4$. θ is the canting angle as shown in (c). (d) shows the top view of (c); φ is the rotation of the in-plane component from the y axis.

We next discuss staggered skew angle defined by $\delta\bar{\phi}^{-} \equiv (\delta\bar{\phi}_{\uparrow} - \delta\bar{\phi}_{\downarrow})/2$ which relates to SHE. Figure 5(a) is the contour plot of $\delta\bar{\phi}^{-}$ when the three spins lie in the xy plane. The result resembles that of the net vector spin chirality of three spins,

$$\begin{aligned}\chi_v =& \mathbf{z}\cdot(\boldsymbol{S}_1\times\boldsymbol{S}_2+\boldsymbol{S}_2\times\boldsymbol{S}_3+\boldsymbol{S}_3\times\boldsymbol{S}_1)\,,\\ =& \sin(\varphi_2-\varphi_1)+\sin(\varphi_3-\varphi_2)+\sin(\varphi_1-\varphi_3),\end{aligned} \quad (11)$$

where $\mathbf{z}$ is the unit vector along the z axis [Fig. 5(b)]. While the result implies a relation between $\delta\bar{\phi}^{-}$ and χ_v, we note that a sum of two-spin scattering cannot produce a finite $\delta\bar{\phi}^{-}$, as we discussed at the end of Sec. II. Hence, we cannot simply attribute the skew scattering to the sum of two-spin scattering proportional to the vector spin chirality.

To gain more insight into the relation between $\delta\bar{\phi}^{-}$ and spin chirality, we rewrite

$$\frac{1}{J\sum_l \vec{S}_l\cdot\vec{\sigma}_l - \Sigma(\varepsilon)} = \sum_{n=0}^{\infty}\left(-G_z H_f\right)^n G_z, \quad (12)$$

which is an expansion valid in the $V/t, J/t \ll 1$ limit. When $S_i^z = 0$, the leading order in asymmetric scattering rate $\bar{\mathcal{W}}^{-}_{\vec{k},\vec{k}'} = (\bar{\mathcal{W}}_{\vec{k}\uparrow,\vec{k}'\uparrow} - \bar{\mathcal{W}}_{\vec{k}\downarrow,\vec{k}'\downarrow})/2$ appears from the $n = 3$ term ($\propto J^3$),

$$\bar{\mathcal{W}}^{-}_{\vec{k},\vec{k}'} \sim \frac{2V^4}{N^2}\sum_{i,m,n}\mathrm{Im}\left[\Sigma_{ii}\Sigma^{*}_{mn}\right](\boldsymbol{S}_m\times\boldsymbol{S}_n)_z J_0\left(k\sqrt{r_{im}^2+r_{in}^2-2\boldsymbol{r}_{im}\cdot\boldsymbol{r}_{in}\cos(\delta\phi)+2(\boldsymbol{r}_{im}\times\boldsymbol{r}_{in})_z\sin(\delta\phi)}\right). \quad (13)$$

Here, we used $\boldsymbol{S}_i\cdot\boldsymbol{S}_i = 1$. This term corresponds to the eighth order in V, in which the electrons are scattered twice by $\boldsymbol{S}_i$ and once by $\boldsymbol{S}_j$ and $\boldsymbol{S}_k$. Hence, the skew scattering requires at least three spins while the skew angle is proportional to the net vector spin chirality, similar to a mechanism involving both spins and nonmagnetic impurity [30].

For the three spin cluster with $\Sigma_{11} = \Sigma_{22} = \Sigma_{33} = \Sigma_d$ and $\Sigma_{12} = \Sigma_{23} = \Sigma_{31} = \Sigma_{od}$, the above formula becomes

$$\bar{\mathcal{W}}^{-}_{\vec{k},\vec{k}'} \sim \frac{2V^4}{N^2}\mathrm{Im}\left[\Sigma_d\Sigma^{*}_{od}\right]\sum_{m,n}(\boldsymbol{S}_m\times\boldsymbol{S}_n)_z\sum_i J_0\left(k\sqrt{r_{im}^2+r_{in}^2-2\boldsymbol{r}_{im}\cdot\boldsymbol{r}_{in}\cos(\delta\phi)+2(\boldsymbol{r}_{im}\times\boldsymbol{r}_{in})_z\sin(\delta\phi)}\right), \quad (14)$$

with the sum over i being independent of m and n. This equation supports the observation in Fig. 5, which relates $\delta\bar{\phi}^{-}$ to vector spin chirality.

V. SPIN-CLUSTER SCATTERING AND SPIN CHIRALITY

To make the observation about skew angles and spin chirality more rigorous, we next look at how the scattering rate $\bar{W}_{\sigma,\sigma'}(\delta\phi)$ changes by changing the canting angle and permuting spins. In particular, we look at how $\bar{W}_{\sigma,\sigma'}(\delta\phi)$ transforms under the following three cases:

1. $\bar{W}_{\sigma,\sigma'}(\delta\phi)|_{\theta} = \bar{W}_{\sigma,\sigma'}(\delta\phi)|_{-\theta}$. — Here, $\bar{W}_{\sigma,\sigma'}(\delta\phi)|_{\theta}$ is the scattering rate for a three spin cluster with canting angle θ; the spins cant outward when $\theta > 0$ [Fig. 1(b)] and inward when $\theta < 0$ [Fig. 1(c)]. We can show this

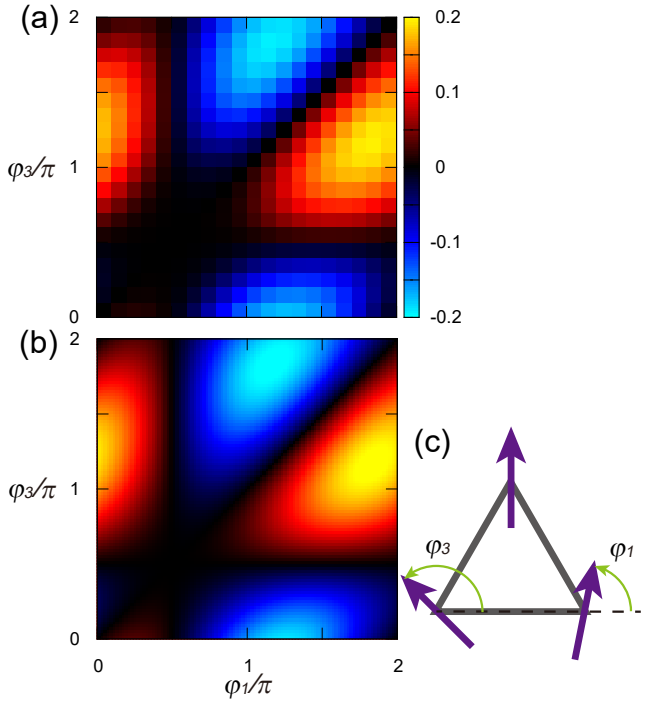

FIG. 5. Spin configuration dependence of the spin-dependent skew angle $\delta\bar{\phi}^-$ when all spins lie in the xy plane. (a) Contour plot of $\delta\bar{\phi}^-/\pi$ calculated using Eq. (7) for $J/t = V/t = 6$, $k_F = 1$, and $\theta = \pi/2$. (b) the net vector chirality χ_v in Eq. (11) with $\varphi_2 = \pi/2$. φ_1 and φ_3 defines the relative angle of spins as in (c).

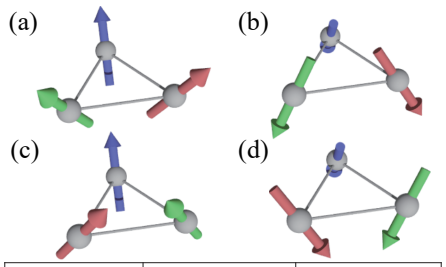

	θ	$\pi-\theta$
clockwise	+ (a) / +	− (b) / +
counter-clockwise	− (c) / −	+ (d) / −

$\delta\phi_+ \equiv (\delta\phi_\uparrow + \delta\phi_\downarrow)/2$
$\delta\phi_- \equiv (\delta\phi_\uparrow - \delta\phi_\downarrow)/2$

FIG. 6. The relation of the sign of average ($\delta\bar{\phi}_+$) and staggered ($\delta\bar{\phi}_-$) to the spin configuration. (a-d) Examples of spin configurations we consider: The clockwise (a,b) or counter-clockwise (c,d) orientation and the canting angle θ (a,c) or $\pi-\theta$ (b,d). The sign of $\delta\bar{\phi}_\pm$ for each configuration is summarized in the bottom table. The upper sign in each block is for $\delta\bar{\phi}_+$ and the lower one is for $\delta\bar{\phi}_-$. The alphabet in each cell shows corresponding spin configuration in (a-d).

property by rewriting Eq. (7) using an expansion,

$$\frac{1}{J\sum_l \vec{S}_l\cdot\vec{\sigma}_l - \Sigma(\varepsilon)} = \sum_{n=0}^{\infty}\left(G_zH'\right)^{2n}G_z - \sum_{n=0}^{\infty}\left(G_zH'\right)^{2n}G_zH'G_z, \quad (15)$$

where $G_z = [J\sum_l S_l^z\sigma_l^z - \Sigma(0)]^{-1}$ and $H' = \sum_l S_l^x\sigma_l^x + S_l^y\sigma_l^y$. The first term of this equation is diagonal in the spin index, while the diagonal elements in the second term are zero. Substituting this formula into Eq. (7), we find

$$\bar{\mathcal{W}}_{\vec{k}\sigma,\vec{k}'\sigma'} = \frac{V^4}{N^2}\sum_{i,j,m,n}\left[\left(G_zH'\right)^{2n}G_z\right]_{i\sigma,j\sigma'}\left[\left(G_zH'\right)^{2n}G_z\right]^*_{m\sigma,n\sigma'} \times J_0\left(k\sqrt{r_{jn}^2 + r_{im}^2 - 2\vec{r}_{im}\cdot\vec{r}_{jn}\cos(\delta\phi) + 2(\vec{r}_{im}\times\vec{r}_{jn})_z\sin(\delta\phi)}\right), \quad (16a)$$

for $\sigma = \sigma'$ and

$$\bar{\mathcal{W}}_{\vec{k}\sigma,\vec{k}'\sigma'} = \frac{V^4}{N^2}\sum_{i,j,m,n}\left[\sum_{n=0}^{\infty}\left(G_zH'\right)^{2n}G_zH'G_z\right]_{i\sigma,j\sigma'}\left[\sum_{n=0}^{\infty}\left(G_zH'\right)^{2n}G_zH'G_z\right]^*_{m\sigma,n\sigma'} \times J_0\left(k\sqrt{r_{jn}^2 + r_{im}^2 - 2\vec{r}_{im}\cdot\vec{r}_{jn}\cos(\delta\phi) + 2(\vec{r}_{im}\times\vec{r}_{jn})_z\sin(\delta\phi)}\right), \quad (16b)$$

for $\sigma \neq \sigma'$. As $G_z \to G_z$ and $H' \to -H'$ under the transformation $\theta \to -\theta$, the scattering rate transforms

$\bar{W}_{\sigma,\sigma'}(\delta\phi) \to \bar{W}_{\sigma,\sigma'}(\delta\phi)$. This property holds for both scalar and vector spin chiralities.

2. $\bar{W}_{\sigma,\sigma'}(\delta\phi)|_c = \bar{W}_{\sigma,\sigma'}(-\delta\phi)|_{cc}$. — Here, $\bar{W}_{\sigma,\sigma'}(\delta\phi)|_c$ and $\bar{W}_{\sigma,\sigma'}(-\delta\phi)|_{cc}$ are respectively the scattering rate for clockwise and counter-clockwise configurations. Formally, the clockwise to counter-clockwise transformation is equivalent to permuting two sites, e.g., $\boldsymbol{r}_1 \leftrightarrow \boldsymbol{r}_3$. We define the switched positions by $\boldsymbol{r}'_l$:

$$\boldsymbol{r}_1 = \boldsymbol{r}'_3, \qquad \boldsymbol{r}_2 = \boldsymbol{r}'_2, \qquad \boldsymbol{r}_3 = \boldsymbol{r}'_1. \tag{17}$$

To make the argument concrete, we set $\boldsymbol{r}_1 = (-1/2, 0)$, $\boldsymbol{r}_2 = (0, \sqrt{3}/2)$, and $\boldsymbol{r}_3 = (1/2, 0)$. In this notation, $\boldsymbol{r}_i \to \boldsymbol{r}'_i$ is equivalent to the mirror operation about x axis: $x \to -x$ and $y \to y$. Therefore, $\boldsymbol{r}_{ij}\cdot\boldsymbol{r}_{nm} = \boldsymbol{r}'_{ij}\cdot\boldsymbol{r}'_{nm}$, $\boldsymbol{r}_{ij}\times\boldsymbol{r}_{nm} = -\boldsymbol{r}'_{ij}\times\boldsymbol{r}'_{nm}$. Therefore, the scattering rate after the transformation reads

$$\begin{aligned}\bar{\mathcal{W}}'_{\sigma,\sigma'}(\delta\phi) =& \frac{V^4}{N^2}\sum_{i,j,m,n}\left[\frac{1}{J\sum_l \boldsymbol{S}_l\cdot\boldsymbol{\sigma}_l - \Sigma(\varepsilon)}\right]_{i\sigma,j\sigma'}\left[\frac{1}{J\sum_l \boldsymbol{S}_l\cdot\boldsymbol{\sigma}_l - \Sigma(\varepsilon)}\right]^*_{m\sigma,n\sigma'} \\ &\times J_0\left(k\sqrt{r_{jn}^2 + r_{im}^2 - 2\boldsymbol{r}_{im}\cdot\boldsymbol{r}_{jn}\cos(-\delta\phi) + 2(\boldsymbol{r}_{im}\times\boldsymbol{r}_{jn})_z\sin(-\delta\phi)}\right), \\ =& \bar{\mathcal{W}}_{\sigma,\sigma'}(-\delta\phi).\end{aligned} \tag{18}$$

This transformation changes the sign of scalar and vector spin chiralities. In the view of $\delta\bar{\phi}_\pm$, this property changes the sign of $\delta\bar{\phi}_+$ and $\delta\bar{\phi}_-$ by transforming the counter-clockwise configuration to clockwise configuration [see the table in Fig. 6].

3. $\bar{W}_{\sigma,\sigma'}(\delta\phi)|_\theta = \bar{W}_{\bar{\sigma},\bar{\sigma}'}(-\delta\phi)|_{\pi-\theta}$. — Here, $\bar{\sigma} = \downarrow, \uparrow$ for $\sigma = \uparrow, \downarrow$. We can show this from the π rotation about the incident momentum $\boldsymbol{k}'$ [Fig. 1(b)]. Suppose $\boldsymbol{k}'$ is parallel to the solid line in Fig. 1(b). Then, the π rotation about this axis and φ_R rotation about the axis perpendicular to the plane transforms the spin cluster with θ to that with $\pi - \theta$. As the π rotation changes $\delta\phi \to -\delta\phi$, we find $\bar{W}_{\sigma,\sigma'}(\delta\phi)|_\theta = \bar{W}_{\bar{\sigma},\bar{\sigma}'}(-\delta\phi)|_{\pi-\theta}$.This transformation changes scalar spin chirality but not vector spin chirality. Regarding $\delta\bar{\phi}_\pm$, the above transformation changes the sign of $\delta\bar{\phi}_+$ while it leaves $\delta\bar{\phi}_-$ invariant [see the table in Fig. 6].

The sign of $\delta\bar{\phi}_\pm$ is summarized in the table on Fig. 6. From the table, we see that $\delta\bar{\phi}_+$ has the same property as scalar spin chirality while $\delta\bar{\phi}_-$ follows that of the vector spin chirality. The same symmetry properties between chirality and $\delta\bar{\phi}_\pm$ support using the chiralities as an indicator for the anomalous Hall effect, even with a strong Kondo coupling.

VI. DISCUSSIONS

To summarize, in this work, we studied the skew scattering of electrons by three-spin clusters using a T-matrix method, going beyond the perturbation limit studied in [24, 30]. Using an Anderson impurity model and the Green-function method, we calculated the scattering rate of the spin clusters for the arbitrary strength of Kondo coupling. We find that the spin cluster causes a skew scattering with a large skew angle, reaching the order of 0.1π rad. This skew angle is 10-100 times larger than other skew scattering mechanisms. Hence, it potentially produces large anomalous and spin Hall effects related to the local spin correlation. The T-matrix formula for scattering rate also shows that the skew angle for AHE and SHE has the same symmetry properties as scalar and vector spin chiralities, respectively. Hence, the chiralities function as an indicator for the Hall effects, even for a large Kondo coupling.

We note that a Kondo resonance mechanism can also produce a large spin Hall angle [52–54]. This phenomenon, however, is unique to SHE in paramagnetic metals because both magnetism and magnetic field suppress Kondo resonance. Therefore, large AHE/SHE in magnetically-ordered phases or under magnetic field is unlikely by the Kondo resonance.

Experimentally, magnetic materials with strong Kondo coupling are known in transition-metal compounds. For example, the double-exchange limit of the Kondo lattice model is considered as the effective model for manganese oxides [8, 35, 42] and chiral magnets forming magnetic skyrmions [43]. In the latter, small-radius skyrmions are expected to appear as the low-energy excitations in the field-induced ferromagnetic state above a skyrmion crystal phase. The canting angle between the neighboring spins at the skyrmion becomes large due to small radius. We also note that a recent experiment on MgZnO/ZnO interface finds a large AHE with Hall angle $> 0.1\pi$ rad and skew-scattering-like scaling [41]. Defects spins are the likely origin of ferromagnetism in ZnO [44–46], which may form a canted spin state due to the interfacial Dzyaloshinskii-Moriya interaction. In a different experiment, a large spin Hall effect was reported in Pd- and Au-based metallic spin glasses [47]. Exchange interactions between the spins are often mediated by long-range Ruderman-Kittel-Kasuya-Yosida (RKKY) interac-

tion [48–50] with the length scale $1/k_F$. As RKKY interaction often forms a structure with a typical length of $1/k_F$, skew scattering might be enhanced in metallic spin glasses. These materials are potential candidates for studying skew scattering in magnetic materials with strong Kondo coupling.

Note: Soon after releasing a preprint of this manuscript, two experimental papers claiming the observation of large Hall angle by spin-cluster scattering [].

Appendix A: T matrix of the magnetic-impurity model

We here review a Green's function formula for calculating T matrix, which is convenient for our study. A similar technique was used to study Anderson impurity models [51]. The formula applies to a general system with two subspaces A and B; the size of the Hilbert spaces are N_A and N_B for A and B, respectively. For the sake of convenience, we note the $N_A \times N_A$ matrix Green function for A subspace as G_A and that for B as G_B; the $N_A \times N_B$ matrix corresponding to the inter-subspace Green function elements of A and B is G_{AB} and the other inter-subspace elements is G_{BA}.

We calculate the T matrix from the Green function. The Dyson equation for Green function reads

$$(\varepsilon \pm \mathrm{i}\delta - H_A)G_A^{\pm} - H'_{AB}G_{BA}^{\pm} = 1, \tag{A1}$$
$$(\varepsilon \pm \mathrm{i}\delta - H_B)G_B^{\pm} - H'_{BA}G_{AB}^{\pm} = 1, \tag{A2}$$
$$(\varepsilon \pm \mathrm{i}\delta - H_A)G_{AB}^{\pm} - H'_{AB}G_B^{\pm} = 0, \tag{A3}$$
$$(\varepsilon \pm \mathrm{i}\delta - H_B)G_{BA}^{\pm} - H'_{BA}G_A^{\pm} = 0. \tag{A4}$$

Here, H_A and H_B are the Hamiltonian matrix within each subspace and H'_{AB} and H'_{BA} are the Hamiltonian elements that connects A and B subspaces. The last equation implies $G_{BA}^{\pm} = G_B^{0\pm}H'_{BA}G_A^{\pm}$, where $G_B^{0\pm} = 1/(\varepsilon \pm \mathrm{i}\delta - H_B)$, is the Green function for the decoupled B subspace (when $H'_{AB} = H'_{BA} = 0$). Substituting this result to Eq. (A1), G_A reads

$$G_A^{\pm} = \frac{1}{(G_A^{0\pm})^{-1} - H'_{AB}G_B^{0\pm}H'_{BA}}, \tag{A5}$$

and hence

$$G_{BA}^{\pm} = G_B^{0\pm}H'_{BA}\frac{1}{(G_A^{0\pm})^{-1} - H'_{AB}G_B^{0\pm}H'_{BA}}. \tag{A6}$$

Similarly, we find

$$G_B^{\pm} = \frac{1}{(G_B^{0\pm})^{-1} - H'_{BA}G_A^{0\pm}H'_{AB}}, \tag{A7}$$

and

$$G_{AB}^{\pm} = G_A^{0\pm}H'_{AB}\frac{1}{(G_B^{0\pm})^{-1} - H'_{BA}G_A^{0\pm}H'_{AB}}. \tag{A8}$$

Using the general property of adjoint matrices, $(A^{\dagger})^{-1} = (A^{-1})^{\dagger}$, $G_{AB}^{\pm}$ reads

$$G_{AB}^{\pm} = \frac{1}{(G_A^{0\pm})^{-1} - H'_{AB}G_B^{0\pm}H'_{BA}}H'_{AB}G_B^{0\pm}, \tag{A9}$$

and

$$G_B^{\pm} = G_B^{0\pm} + G_B^{0\pm}H'_{BA}\frac{1}{(G_A^{0\pm})^{-1} - H'_{AB}G_B^{0\pm}H'_{BA}}H'_{AB}G_B^{0\pm}. \tag{A10}$$

Here, we defined the decoupled Green function for A (G_A^0) in a similar manner to G_B^0. The comparison of Eq. (A10) to the T matrix representation, $G_B = G_B^0 + G_B^0 T G_B^0$, implies

$$T = H'_{BA}\frac{1}{(G_A^{0\pm})^{-1} - H'_{AB}G_B^{0\pm}H'_{BA}}H'_{AB}. \tag{A11}$$

This is the general formula for the T matrix of B subspace treating A as the scatterer.

ACKNOWLEDGMENTS

We thank Y. Fujishiro, N. Kanazawa, D. Maryenko, and Y. Tokura for fruitful discussions. This work was supported by JSPS KAKENHI Grant Numbers JP18H04222, JP18H03676, and JP19K14649, and JST CREST Grant Numbers JPMJCR16F1 and JPMJCR1874.

[1] N. Nagaosa, J. Sinova, S. Onoda, A. H. MacDonald, & N. P. Ong, Rev. Mod. Phys. **82**, 1539-1592 (2010).

[2] J. Sinova, S. O. Valenzuela, J. Wunderlich, C. H. Back, & T. Jungwirth, Rev. Mod. Phys. **87**, 1213-1259 (2015).

[3] S. Maekawa, S. O. Valenzuela, E. Saitoh, & T. Kimura, *Spin current* 2ed. (Oxford Univ. Press, Oxford, 2017).

[4] R. Karplus & J. M. Luttinger, Phys. Rev. **95**, 1154-1160 (1954).

[5] D. Xiao, M.-C. Chang, & Q. Niu, Rev. Mod. Phys. **82**, 1959-2007 (2010).

[6] S. Murakami, N. Nagaosa, & S.-C. Zhang, Science **301**, 1348-1351 (2003).

[7] J. Sinova,, D. Culcer, Q. Niu, N. A. Sinitsyn, T. Jungwirth, & A. H. MacDonald, Phys. Rev. Lett. **92**, 126603 (2004).
[8] J. Ye, Y.-B. Kim, A. J. Millis, B. I. Shraiman, P. Majumdar, & Z. Tesanovic, Phys. Rev. Lett. **83**, 3737-3740 (1999).
[9] K. Ohgushi, S. Murakami, & N. Nagaosa, Phys. Rev. B **62**, 6065-6068(R) (2000).
[10] R. Shindou & N. Nagaosa, Phys. Rev. Lett. **87**, 116801 (2001).
[11] Y. Taguchi, Y. Oohara, H. Yoshizawa, N. Nagaosa, & Y. Tokura, Science **291**, 2573-2576 (2001).
[12] S. Nakatsuji, N. Kiyohara, & T. Higo, Nature **527**, 212-215 (2015).
[13] A. Neubauer, C. Pfleiderer, B. Binz, A. Rosch, R. Ritz, P. G. Niklowitz, & P. Boni, Phys. Rev. Lett. **102**, 186602 (2009).
[14] N. Kanazawa, Y. Onose, T. Arima, D. Okuyama, K. Ohoyama, S. Wakimoto, K. Kakurai, S. Ishiwata, & Y. Tokura, Phys. Rev. Lett. **106**, 156603 (2011).
[15] J. Smit, Physica **24**, 3951 (1958).
[16] L. Berger, Phys. Rev. B **2**, 4559-4566 (1970).
[17] J. Kondo, Prog. Theor. Phys. **27**, 772-792 (1962).
[18] A. Fert & P. M. Levy, Phys. Rev. B **36**, 1907-1916 (1987).
[19] K. Yamada, H. Kontani, H. Kohno, Prog. Theor. Phys. **89**, 1155-1166 (1993).
[20] M. I. D'yakonov & V. I. Perel, Phys. Lett. A **35**, 459-469 (1971).
[21] J. E. Hirsch, Phys. Rev. Lett. **83**, 1834-1837 (1999).
[22] T. Miyasato, N. Abe, T. Fujii, A. Asamitsu, S. Onoda, Y. Onose, N. Nagaosa, & Y. Tokura, Phys. Rev. Lett. **99**, 086602 (2007).
[23] S. Onoda, N. Sugimoto, & N. Nagaosa, Phys. Rev. B **77**, 165103 (2008).
[24] G. Tatara & H. Kawamura, J. Phys. Soc. Jpn. **71**, 2613-2616 (2002).
[25] Denisov, K. S., Rozhansky, I. V., Averkiev, N. S. & Lahderanta, E. Electron scattering on a magnetic skyrmion in the nonadiabatic approximation. Phys. Rev. Lett. **117**, 027202 (2016).
[26] Ishizuka, H. & Nagaosa, N. Spin chirality induced skew scattering and anomalous Hall effect in chiral magnets. Sci. Adv. **4**, eaap9962 (2018).
[27] Taguchi, K. & Tatara, G. Anomalous Hall conductivity due to vector spin chirality in the weak coupling regime. Phys. Rev. B **79**, 054423(R) (2009).
[28] Yi, S.-D., Onoda, S., Nagaosa, N. & Han, J.-H. Skyrmions and anomalous Hall effect in a Dzyaloshinskii-Moriya spiral magnet. Phys. Rev. B **80**, 054416 (2009).
[29] Zhang, D., Ishizuka, H., Lu, N., Wang, Y., Nagaosa, N., Yu, P. & Xue, Q.-K. Anomalous Hall effect and spin fluctuations in ionic liquid gated $SrCoO_3$ thin films. Phys. Rev. B **97**, 184433 (2018).
[30] Ishizuka, H. & Nagaosa, N. Impurity-induced vector spin chirality and anomalous Hall effect in ferromagnetic metals. New J. Phys. **20**, 123027 (2018).
[31] H. Ishizuka & Y. Motome, Phys. Rev. B **87**, 081105(R) (2013).
[32] G.-W. Chern, A. Rahmani, I. Martin, & C. D. Batista, Phys. Rev. B **90**, 241102(R) (2014).
[33] H. Ishizuka & Y. Motome, Phys. Rev. B **88**, 100402(R) (2013).
[34] C. Zener, Phys. Rev. **82**, 403-405 (1951).
[35] P. W. Anderson & A. Hasegawa, Consideration on double exchange. Phys. Rev. **100**, 675-681 (1955).
[36] J. Iwasaki, A. J. Beekman, & N. Nagaosa, Phys. Rev. B **89**, 064412 (2014).
[37] Y. Aharonov & D. Bohm, Phys. Rev. **115**, 485-491 (1959).
[38] R. A. Brown, J. Phys. A: Math. Gen. **18**, 2497-2508 (1985).
[39] R. A. Brown, Phys. A: Math. Gen. **20**, 3309-3326 (1987).
[40] See Supplemental Material at [URL will be inserted by publisher] for the calculation of anomalous and spin Hall angles, which we calculate using a variational method [57–60].
[41] D. Maryenko, A. S. Mishenko, M. S. Bahramy, A. Ernst, J. Falson, Y. Kozuka, A. Tsukazaki, N. Nagaosa, & M. Kawasaki, Nat. Commun. **8**, 14777 (2017).
[42] C. Zener, Phys. Rev. **82**, 403-405 (1951).
[43] N. Nagaosa & Y. Tokura, Nat. Nanotech. **8**, 899 (2013).
[44] S. Banerjee, M. Mandal, N. Gayathri, & M. Sardar, Appl. Phys. Lett. **91**, 182501 (2007).
[45] N. H. Hong, J. Sakai, & V. J. Brizé, Phys.: Condens. Matter **19**, 036219 (2007).
[46] Q. Xu, H. Schmidt, L. Hartmann, H. Hochmuth, M. Lorenz, A. Setzer, P. Esquinazi, C. Meinecke, & M. Grundmann, Appl. Phys. Lett. **91**, 092503 (2007).
[47] W. Jiao, D. Z. Hou, C. Chen, H. Wang, Y. Z. Zhang, Y. Tian, Z. Y. Qiu, S. Okamoto, K. Watanabe, A. Hirata, T. Egami, E. Saitoh, & M. W. Chen, preprint at https://arxiv.org/abs/1808.10371 (2018).
[48] M. A. Ruderman & C. Kittel, Phys. Rev. **96**, 99-102 (1954).
[49] T. Kasuya, Prog. Theor. Phys. **16**, 45-57 (1956).
[50] K. Yosida, Phys. Rev. **106**, 893-898 (1957).
[51] A. C. Hewson, *The Kondo Problem to Heavy Fermions* (Cambridge Univ. Press, Cambridge, 1993).
[52] Y. Niimi, Y. Kawanishi, D. H. Wei, C. Deranlot, H. X. Yang, M. Chshiev, T. Valet, A. Fert, & Y. Otani, Phys. Rev. Lett. **109**, 156602 (2012).
[53] D. V. Fedorov, C. Herschbach, A. Johansson, S. Ostanin, I. Mertig, M. Gradhand, K. Chadova, D. Kodderitzsch, & H. Ebert, Phys. Rev. B **88**, 085116 (2013).
[54] B. Gu, Z. Xu, M. Mori, T. Ziman, & S. Maekawa, J. Appl. Phys. **117**, 17D503 (2015).
[55] S.-Y. Yang, Y. Wang, B. R. Ortiz, D. Liu, J. Gayles, E. Derunova, R. Gonzalez-Hernandez, L. Smejkal, Y. Chen, S. S. P. Parkin, S. D. Wilson, E. S. Toberer, T. McQueen, M. N. Ali, Sci. Adv. **6**, eabb6003 (2020).
[56] Y. Fujishiro, N. Kanazawa, R. Kurihara, H. Ishizuka, T. Hori, F. S. Yasin, X. Yu, A. Tsukazaki, M. Ichikawa, M. Kawasaki, N. Nagaosa, M. Tokunaga, & Y. Tokura, Nat. Commun. **12**, 317 (2021).
[57] M. Kohler, Z. Phys. **124**, 772 (1948).
[58] E. H. Sondheimer, Proc. Roy. Soc. (London) A **203**, 75 (1950).
[59] J. M. Ziman, "Electrons and Phonons" (Oxford Univ. Press, London, 1960).
[60] A. Fert, J. Phys. F: Met. Phys. **3**, 2126 (1973).